DESIGN OF A RETROFIT CONVERTER FOR AN AMPLIDYNE SYSTEM

A Project Report

submitted by

G. MADHURI

in partial fulfilment of the requirements

for the award of the degree of

BACHELOR OF TECHNOLOGY

&

MASTER OF TECHNOLOGY

DEPARTMENT OF ELECTRICAL ENGINEERING

INDIAN INSTITUTE OF TECHNOLOGY MADRAS

May 15, 2013

CERTIFICATE

This is to certify that the project report titled **DESIGN OF A RETROFIT CONVERTER FOR AN AMPLIDYNE SYSTEM**, submitted by **G. Madhuri**, to the Indian Institute of Technology, Madras, for the award of the degree of **Dual Degree (B.Tech & M.Tech)**, is a bona fide record of the project work done by her under our supervision. The contents of this report, in full or in parts, have not been submitted to any other Institute or University for the award of any degree or diploma.

Dr. Krishna Vasudevan
Research Guide
Professor
Dept. of Electrical Engineering
IIT-Madras, 600 036

Place: Chennai

Date:

ACKNOWLEDGEMENTS

My first and foremost thanks to the Lord Almighty. It is only by His Grace that this project has been successfully completed.

My immense heartfelt thanks to my guide Dr. Krishna Vasudevan, Professor, Department of Electrical Engineering, for his guidance, encouragement, great patience and tolerance. His innovative problem solving techniques have instilled great interest in me in the area of electrical engineering.

I am greatly thankful to Mrs. Jeyasutha and Mr. Kothandraman for their unceasing support, help and encouragement.

I am also thankful to all my labmates, especially, Ms. Ashwathi, Mr. Brahmendra, Mrs. Jeshma, Mrs. Kalai Selvi, Mr. Kedarnath, Mr. Lokesh, Mrs. Poongothai, Mr. Ramesh Babu, Mr. Ravi Teja and Mr. Sandeep for extending their help and counsel, despite their busy schedules.

I am also thankful to my mother for all her love, support and encouragement.

Last, but not the least, I'm thankful to the department, my batchmates and all my professors here. The five year stay at IIT wasn't easy, but they ensured that it was far more enjoyable than what I'd hoped for.

Ad Majorem Dei Gloriam

ABSTRACT

KEYWORDS: Rotary converters; Solid-state converters; Cross-field principle; Amplidyne; Four-quadrant operation.

The rotary converters that had gained a huge importance in the first half of the last century are now losing out to solid-state converters on grounds of efficiency. In present times, when there is a big hype about conserving energy and using power efficiently, we can understand clearly where the future lies, with solid-state converters. It would take a few more decades to completely replace rotary converters, especially in naval and aerospace fields, while the replacement in other fields is rapidly progressive.

The goal of the project was to design a retrofit converter to serve as a replacement for an amplidyne rotary converter system. The resultant converter must achieve controlled four-quadrant operation for the given DC motor, constrained by certain specifications. The motor would be operated at voltages higher than the input voltage therefore stepping it up was compulsory. Different approaches were studied and a final circuit topology was arrived at.

The control systems were suitably designed for achieving control over various parameters and desirable performance. These can be implemented now in TMS320F2812 digital signal processor.

Various simulations were carried out in Simulink to verify the proposed model and to fine tune its performance. Magnetic components, i.e., inductors and transformers, were designed, and the design is subject to hardware verification. PCB designing was done using DipTrace, and the PCB boards were obtained after fabrication. Suitable semiconductor devices were identified and procured.

The amplidyne system can now be replaced with the proposed system, given the board be verified for its functionality which is the near-future scope of this work.

TABLE OF CONTENTS

LIST OF TABLES

LIST OF FIGURES

CHAPTER 1

INTRODUCTION

1.1 Historical Background

There is a famous Latin saying that goes like, *Tempora mutantur, nos et mutamur in illis*, meaning *Times change, and we change with them*. True to this, the field of Electrical Engineering has witnessed several revolutionary changes since its conception. But one of the most significant events is inarguably the **War of Currents** that changed the then conventional DC transmission system into the present AC transmission system. With electricity supplies in their infancy, much depended on choosing the right technology to power homes and businesses and with each side debating the advantages and disadvantages of their systems, it wasn't an easy task. We know who emerged as the victor - AC system.

But while AC system was perfectly adequate for the needs of that century, it simply wasn't for the later years. Time had already tested and verified the advantages of the individual systems circumstantially. This led to a power network that increasingly evolved into a hybrid of AC and DC systems. It was no more a question of AC versus DC, but AC and DC. Consequently, the field of power converters, to convert power from one form to the other, received great interest and research.

With this brief background in picture, the converters developed till date can be classified broadly into two major categories:

1. Rotary converters.
2. Solid-state converters.

1.2 Rotary Converter

A rotary converter is essentially a motor-generator set, which acts as a mechanical rectifier or inverter. It was used for AC/DC conversion (and vice versa) before the advent

of chemical or solid state power rectification. They were commonly used to provide DC power for commercial, industrial and railway electrification from an AC power source. The block diagram is as shown in Figure 1.1.

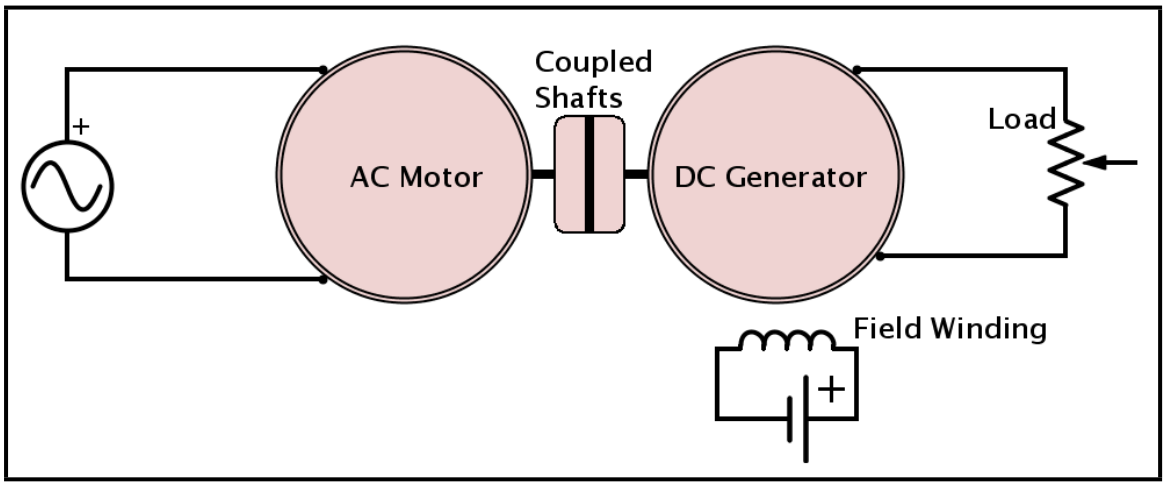

Figure 1.1: Block Diagram of a Rotary Converter

1.2.1 Advantages

1. The set is robust and can work in harsh conditions.
2. It operates at high power factor.
3. The running and operating cost is low.

1.2.2 Disadvantages

1. It is liable to reversal of polarity.
2. Its bulky construction makes the logistics difficult.
3. DC voltage regulation is limited.

1.3 Solid-State Converter

As the name suggests, a solid-state converter is exactly that, converter made using solid-state devices. Different soild-state devices can be used suitably in different topologies to get rectifiers, inverters or step-up and step-down converters. The block diagram is as shown in Figure 1.2.

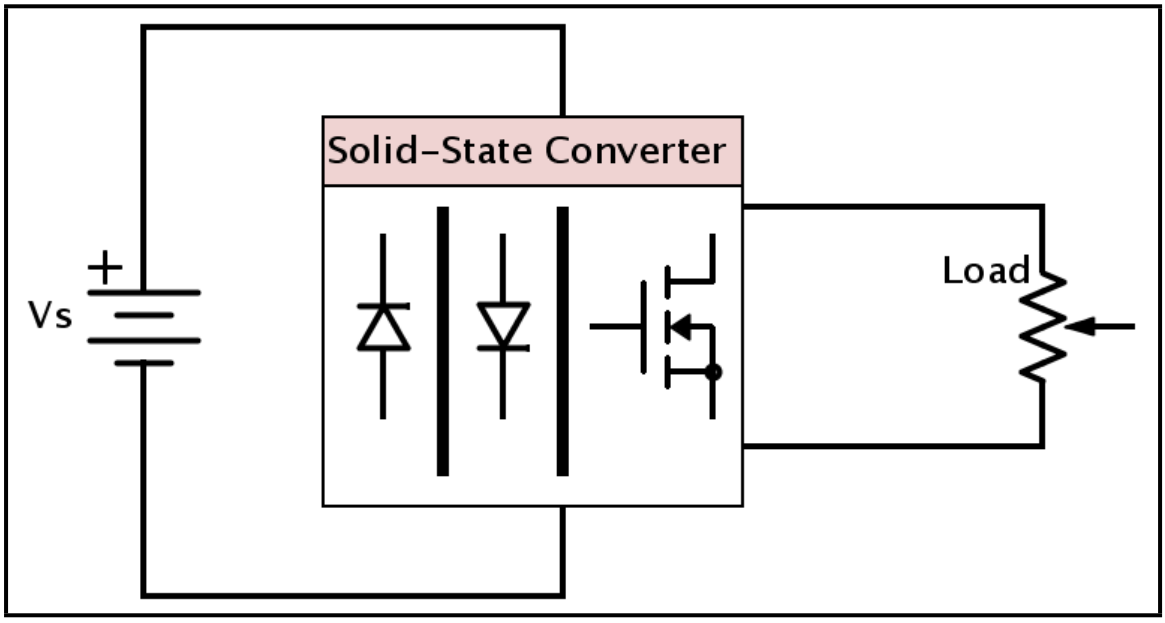

Figure 1.2: Block Diagram of a Solid-State Converter

1.3.1 Advantages

1. It has a fast response due to the semiconductor theory involved in it.
2. It has high efficiency, greater than 90%.
3. Due to advancements in semiconductor technology, converters can be made smaller and are easily transportable.

1.3.2 Disadvantages

1. It cannot operate efficiently in harsh conditions and may collapse.
2. The converter cannot withstand overloading even for few seconds, and the devices may burn.
3. It requires extracting isolated power supplies, thereby increasing the number of components.

1.4 Scope of the project

A brief outline of the two major classes of converters was given in the previous sections. As it currently stands, the solid-state converters are steadily replacing rotary converters, wherever possible, given their many advantages. This work deals with the replacement

of one such rotary converter system, called amplidyne, with a solid-state converter capable of achieving controlled four-quadrant operation.

- *Chapter 2* explains the construction and working of amplidynes.
- The simulation results are analyzed in *Chapter 4*.
- Hardware implementation details are given in *Chapter 5*.
- The conclusions of the work are presented in *Chapter 6*.

CHAPTER 2

AMPLIDYNE

2.1 Cross-field principle

Consider a conventional two-pole DC machine with armature and brushes combination as shown in Figure 2.1.

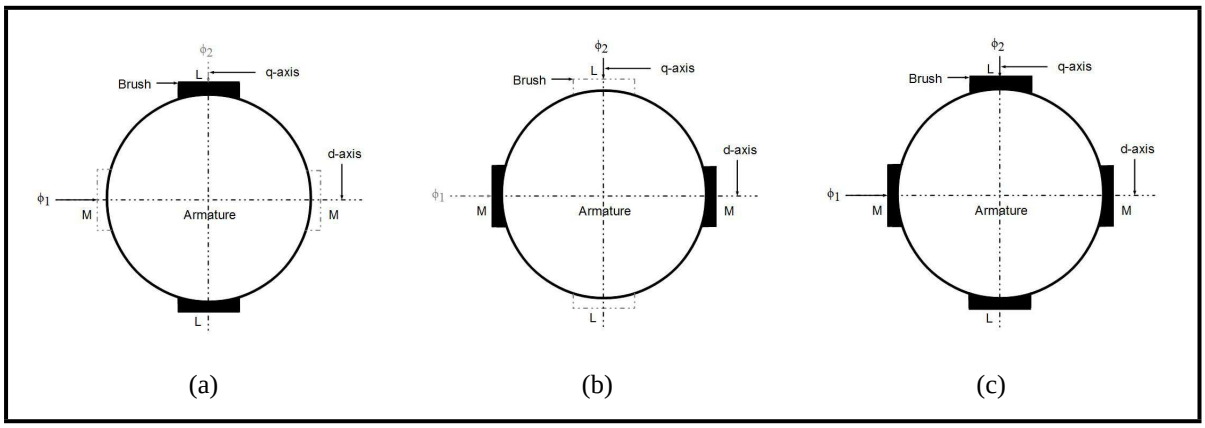

Figure 2.1: Conventional two-pole DC machine with armature and brushes combination

- Refer Figure 2.1(a).
  Flux ϕ_1 along the horizontal axis will generate a voltage between the brushes L and L on the commutator but no voltage between the brushes M and M placed along the field axis (or d-axis) on load. Thus field axis and voltage axis are at right angles.

- Refer Figure 2.1(b).
  Flux ϕ_2 along the vertical axis will generate voltage between brushes M and M placed along horizontal axis, on the commutator but no voltage will be induced between brushes L and L placed along the vertical axis.

- Refer Figure 2.1(c).
  The above-mentioned cases are now combined. Flux ϕ_1 along the horizontal axis generates voltage V_{LL} and flux ϕ_2 along the vertical axis induces voltage V_{MM} and neither the fluxes nor the voltages interfere with each other. Thus, this device is *virtually two machines in one*, if armature reaction is negligible or full compensation is provided. Although the currents are superimposed in the same armature conductors, they can still be considered to have a separate existence. This leads to an interconnection between the two systems which is made use of in machines called **cross-field generators**.

2.2 The Rosenberg Generator

The Rosenberg generator was originally used as a train-lighting generator. This was fore-runner of the cross-field machines from which the amplidyne and other types of metadynes were developed later on. Its properties were:

1. It develops an emf in the direction which is independent of the direction of rotation.
2. It produces a current, which, beyond a certain speed, remains practically constant.

The connections are as shown in Figure 2.2.

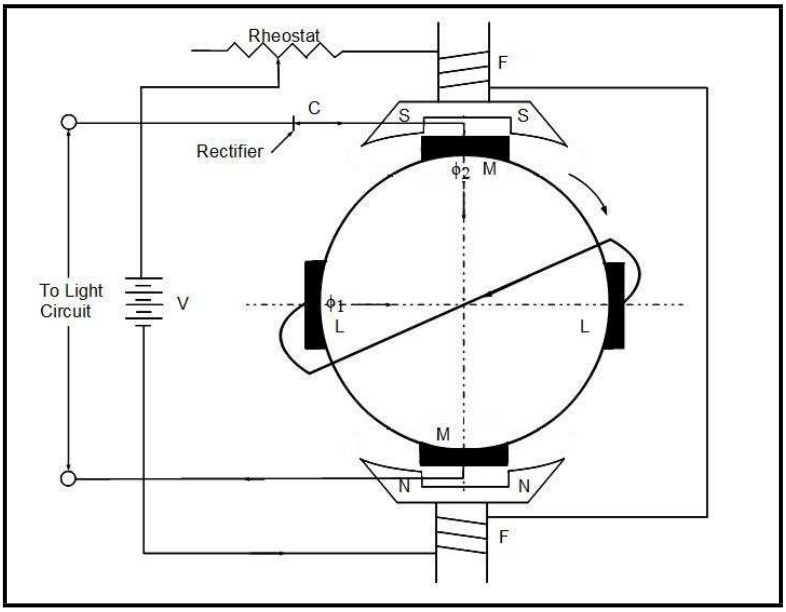

Figure 2.2: Rosenberg train-lighting generator

2.2.1 Components

- The battery V supplies current to the lamp when the train is at rest and also to the shunt field winding FF, producing the polarity as indicated by NN, SS. The axis of commutation of the brushes MM is in line with the axis of the poles.
- The brushes MM are connected to the battery terminals through a rectifier element which blocks the flow of current from the battery to the armature, but maintains it by offering a low resistance path in the other direction.
- In addition to the main set of brushes, there is a pair of short-circuited auxiliary brushes LL, placed at right angles to the field axis.

2.2.2 Working

- When the armature windings rotate through the magnetic field setup by FF, a current is produced which flows through the short-circuited armature brush set LL, creating the field ϕ_1. The clockwise rotation results in a field that is directed from left to right. The rotation of the armature windings through this cross-field generates an emf and current along the MM axis in the direction along ϕ_2, such that it opposes the main excitation created by FF. With the direction of rotation reversed, the direction of the cross-field ϕ_1 also reverses, preserving the original polarity across the brushes MM. Since ϕ_2 opposes the excitation due to the field winding, the net field flux parallel to the MM axis is small, ensuring there is not excessive current flowing through the short-circuited LL.
- Thus, there is a definite current limit deliverable by the brushes MM, by virtue of its construction. This is reached when ϕ_2 neutralizes the field excitation due to FF.There would be no further emf and current in the LL axis, and hence no emf in the main brush.

As seen in the case of Rosenberg generator, there was no compensation provided for the armature reaction mmf set up by the load current. In one way, this was essential for giving constant current characteristics. Amplidynes and metadynes are machines that have evolved from Rosenberg generators and have a compensating winding in series with the power output brush terminals to neutralize this armature reaction mmf. Fully compensated machine is called the amplidyne, while the under compensated machine is called the metadyne.

2.3 Amplidyne

The amplidyne is an electromechanical amplifier with a high DC power gain and a relatively rapid response.

2.3.1 Working

Consider a conventional DC generator as shown in Figure 2.3. The control field excitation power that it requires, is nearly 1% of its rated output power. Therefore, here the separately excited DC generator system may be considered as a rotary power amplifier. Infact, any generator, may be considered as a rotary amplifier.

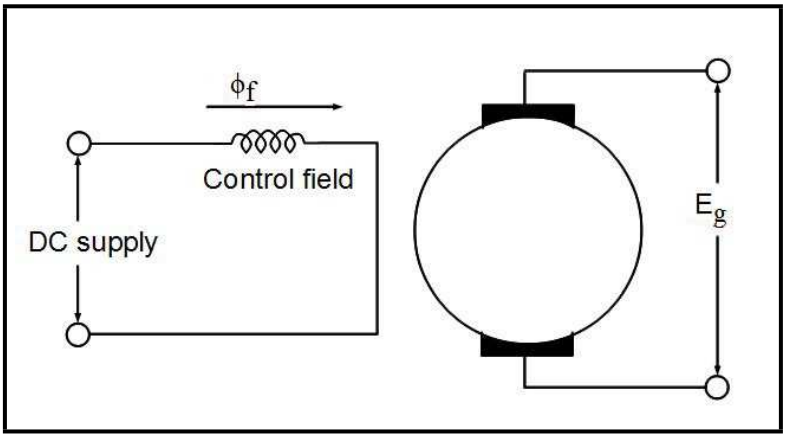

Figure 2.3: Separately excited generator

Now consider the same generator with its armature terminals shorted as shown in Figure 2.4. Now, to operate on the rated load without damaging the generator, it is necessary to reduce the field excitation to let us say, one hundredth of its original excitation. The rated short-circuit armature current produces an armature reaction flux ϕ_{a1}. Assuming that this field is of the same magnitude as the field flux, the same voltage, E_a, is now generated across the brushes placed across the cross-field. Thus, one hundredth of the original excitation is capable of operating on the same load as earlier.

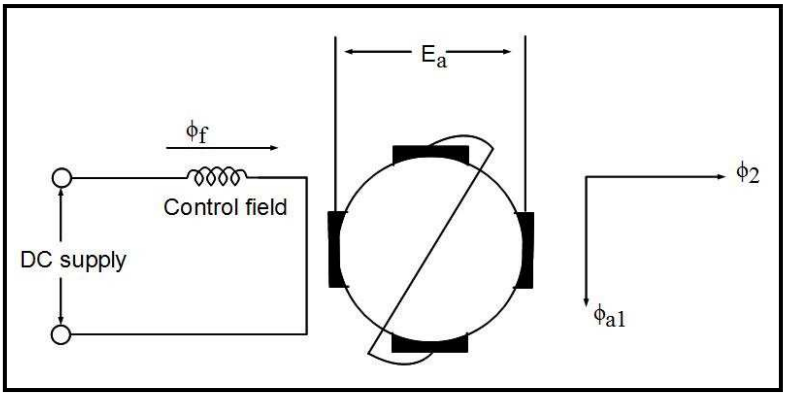

Figure 2.4: Quadrature field

Figure 2.5(a) shows the system with a load connected across the cross-field axis brushes, and the phasor diagram of the fluxes is as shown in Figure 2.5(b). The armature conductors produce a flux ϕ_{a2} directly in opposition to the control field, ϕ_f. It is highly undesirable to have the quadrature armature reaction result from this, because it would oppose the main field and give a strong negative feedback, limiting the output of the amplidyne. A compensating winding, is therefore connected, as shown in Figure 2.5(a),

whose flux is in the same direction as the control field and whose mmf varies with the load current. Therefore, the arrangement is such that under all load conditions, the load current flux ϕ_{a2} is always neutralized by the compensating flux ϕ_c, as shown in Figure 2.5(b).

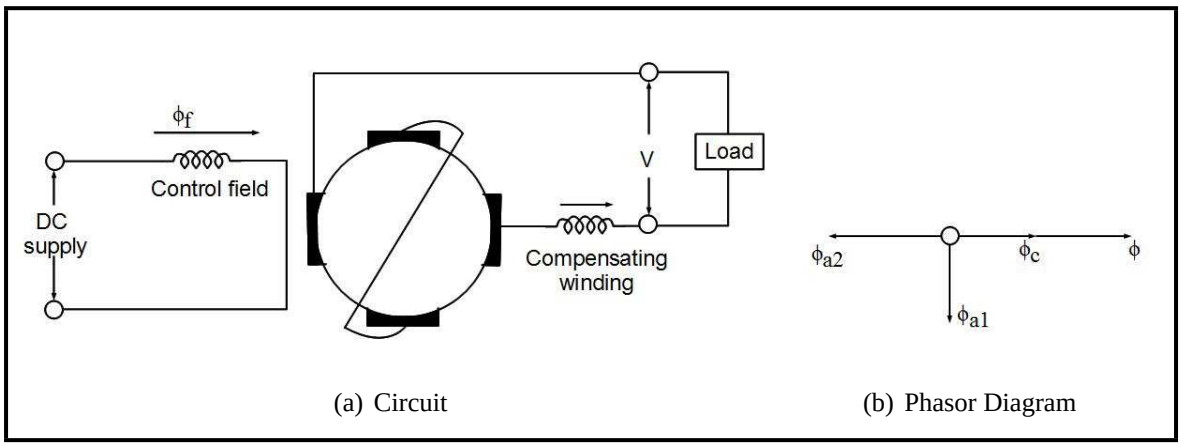

(a) Circuit (b) Phasor Diagram

Figure 2.5: With compensations windings

Therefore, the amplidyne is clearly seen to be a variation of the conventional motor-generator set, in that it uses its own armature excitation. the response is relatively faster than having two separate machines, and the size is reduced to half too.

CHAPTER 3

SIMULATIONS

3.1 Amplidyne Characteristics

The amplidyne to be replaced acts as a current source, by virtue of construction, as shown in Figure 3.1.

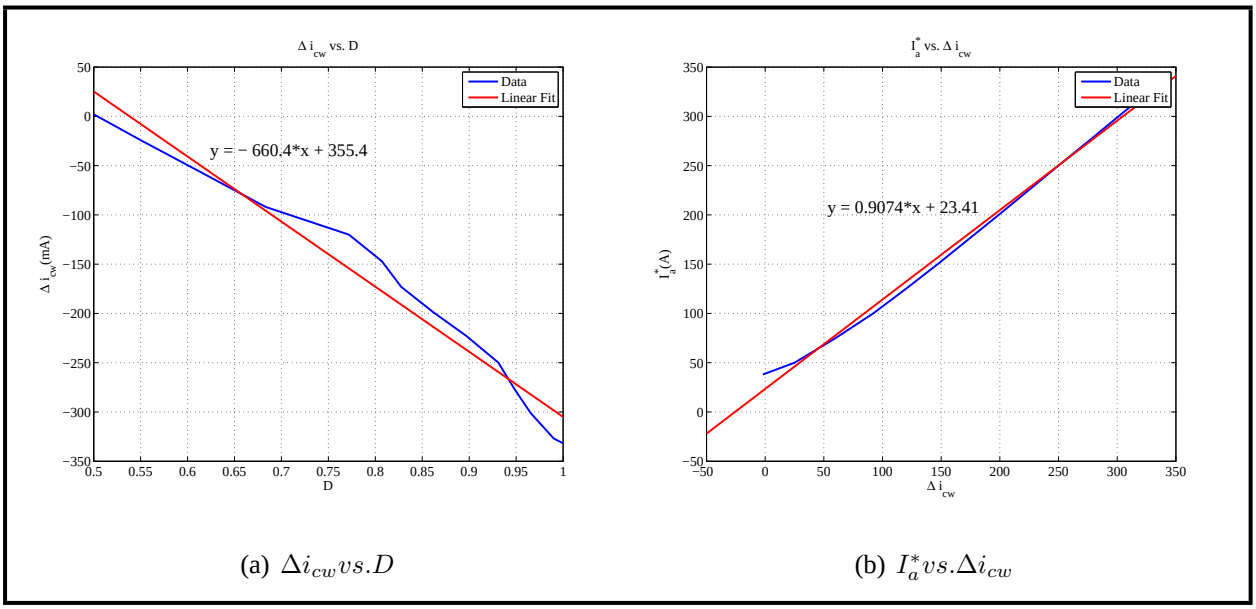

(a) $\Delta i_{cw} vs. D$ (b) $I_a^* vs. \Delta i_{cw}$

Figure 3.1: Amplidyne Characteristics

The simulations have been carried out for a typical industrial system, whose specifications are as given in Table 3.1:

Table 3.1: Motor Parameters

N_{rated}	2000rpm
V_{rated}	115V
P_{rated}	2kW
R_a	0.65Ω
L_a	5mH
J	0.032kg.m^2
B_m	10μN.m.s
R_f	115Ω
L_f	11.5H
L_{af}	0.4H

The optimum input voltage available to the system is $V_{input} = 22V$. This could vary in the range $18V - 27V$. Since $V_{input} > V_{rated}$, there is clearly a need for stepping up the voltage. The approach is discussed in the following sections.

3.2 Initial Approach

The circuit diagram is as shown in Figure 3.2.

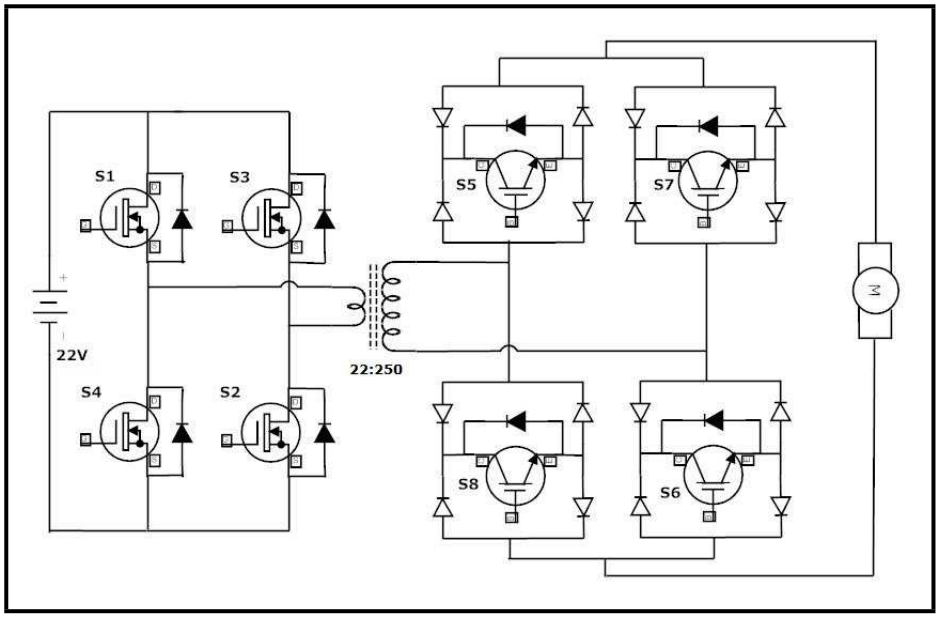

Figure 3.2: Initial Approach

3.2.1 Working

The H-bridge inverter at the primary of the transformer converts the DC input voltage into an AC wave. The turns ratio of the transformer is $22 : 250$. The switches and the diodes at the secondary of the transformer are operated such that the four-quadrant operation is achieved.

The switching waveforms for the switch pairs $S1, S2$ and $S3, S4$, and the resultant voltage waveforms at the primary and secondary of the transformer are as shown in Figure 3.3.

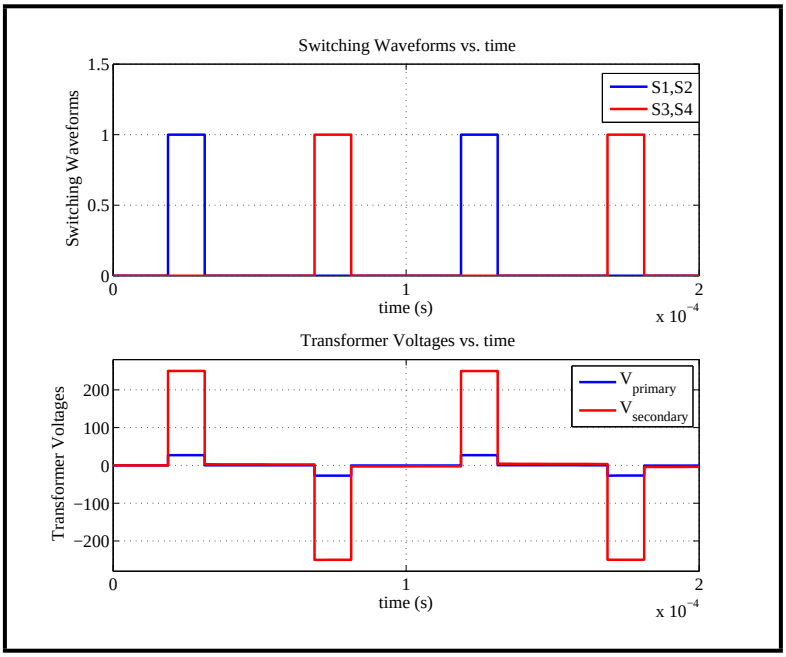

Figure 3.3: Input Bridge: Switching Waveforms and Resultant Voltages

For the output bridge, the switching waveforms for positive output voltages and negative output voltages are as shown in Figure 3.11(a) and Figure 3.11(b), respectively.
For positive output voltages:

- $S5 : S1, S2$
- $S6 : \bar{S3}, \bar{S4}$
- $S7 : \bar{S1}, \bar{S2}$
- $S8 : S3, S4$

For negative voltages:

- $S5 : S3, S4$
- $S6 : \bar{S1}, \bar{S2}$
- $S7 : \bar{S3}, \bar{S4}$
- $S8 : S1, S2$

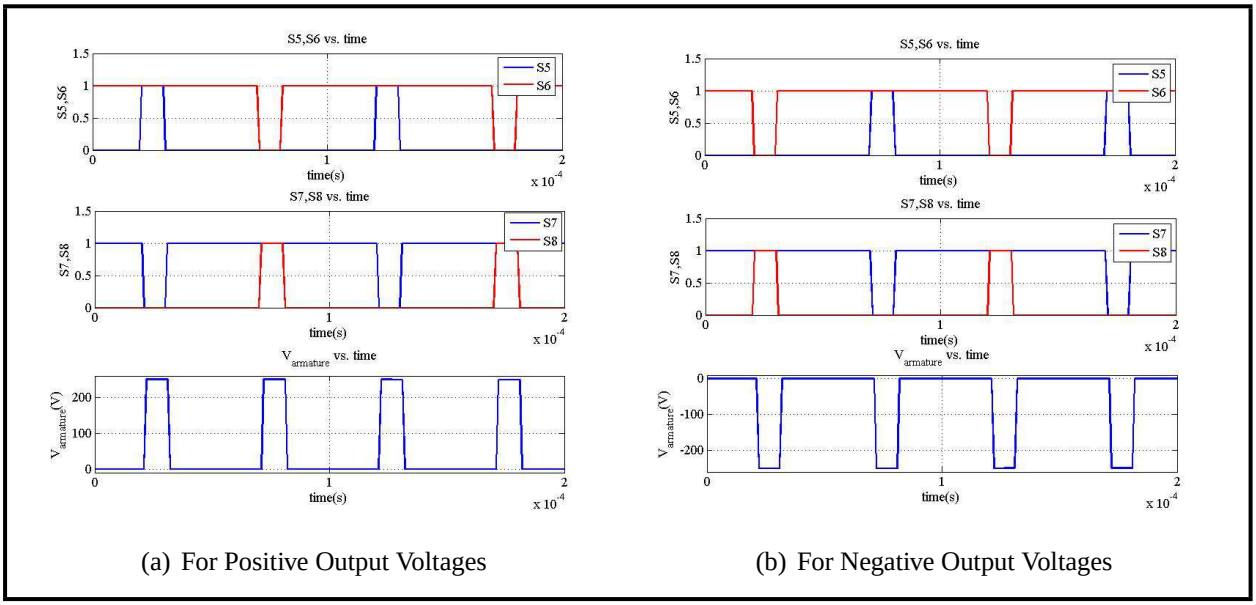

(a) For Positive Output Voltages (b) For Negative Output Voltages

Figure 3.4: Output Bridge: Switching Waveforms

This scheme was arrived at after considerable investigation of the system. The requirement is that the resultant voltage waveform be strictly unipolar in one period of operation, not bipolar (i.e., not changing from $+V_c$ to $-V_c$, and vice-versa; but changing from 0 to $+/-V_c$, and vice-versa), and this scheme provides exactly that.

3.2.2 Control System

The control system implemented is as shown in Figure 3.5. The motor armature current, I_a(A) is fed into the inner loop, while the motor speed, ω_m(rad/s) is fed into the outer loop.

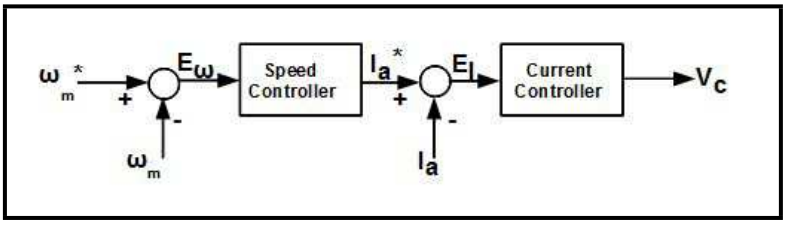

Figure 3.5: Control Loop

The blocks *Speed Controller* and *Current Controller* are PI controllers implemented as shown in Figure 3.6.

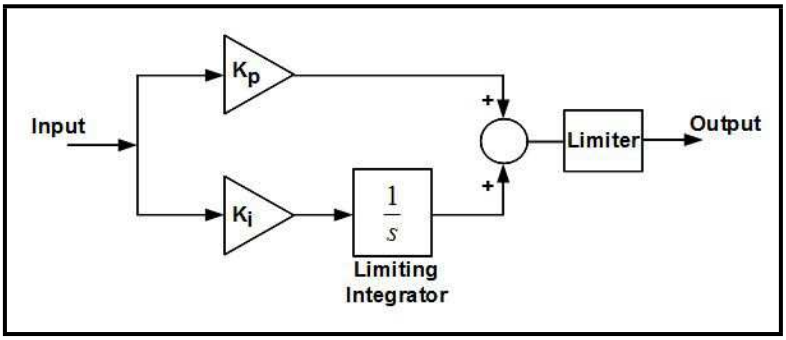

Figure 3.6: PI Controller

The values for the K_p and K_i for the speed and current controllers are determined from bode plots of the respective plant transfer functions.

The output signal from control system, V_c, is limited between $-10V$ and $10V$. This is compared with a bipolar triangle wave (peak-peak value of $20V$) for switch pair $S1, S2$. For the switch pair $S3, S4$, $-V_c$ is compared. These comparisons then generate switching pulses with different duty ratios, depending on the value of V_c, hence controlling the system according to our requirements. This is as shown in Figure 3.7.

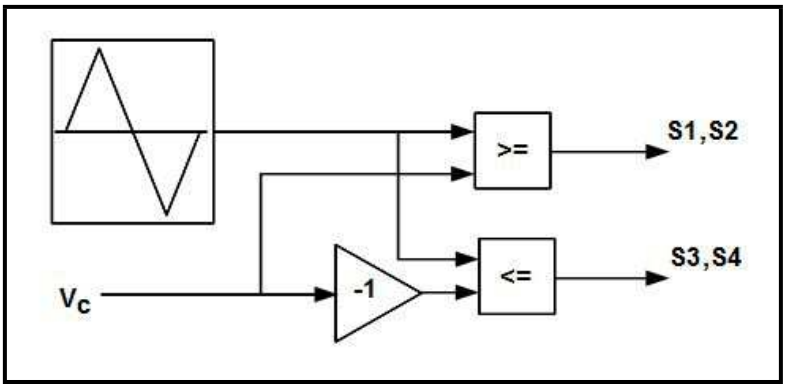

Figure 3.7: Switching Scheme

3.2.3 Disadvantage

Despite satisfactory performances offered by the power and control systems, this topology was rejected because the steady state current drawn under even the most optimum loading conditions on the input side of the transformer was $300A$, which, under certain loading condition rose up to $750A$. Therefore the hardware implementation of this topology would be problematic since many devices would have to be put in parallel to

carry this current, resulting in a large area of occupation by the entire system.

3.3 Working Topology

The circuit diagram is as shown in Figure 3.8.

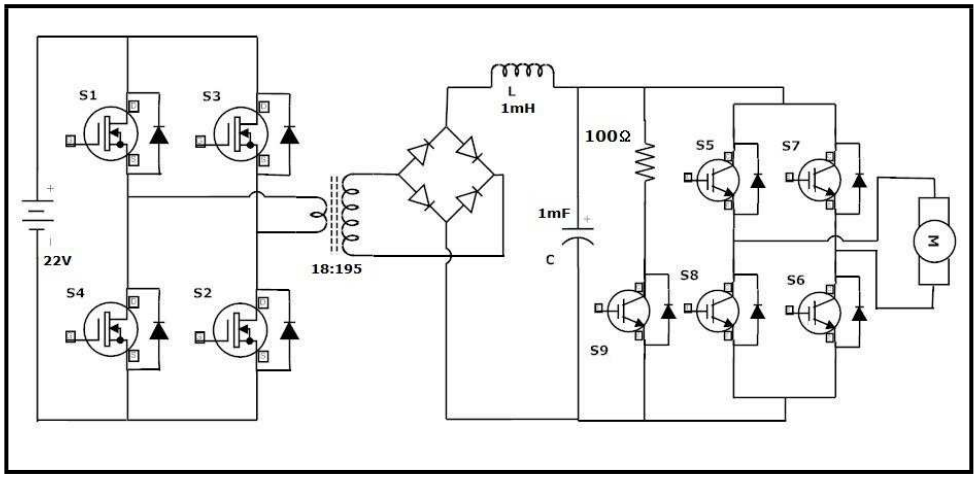

Figure 3.8: Working Topology: Circuit Diagram

3.3.1 Working

The H-bridge inverter on the primary side of the transformer has the same functionality as earlier, converting the DC input voltage into an AC wave. The turns ratio of the transformer is $18:195$. The diode rectifier at the secondary of the transformer rectifies this AC wave and the LC lowpass filter filters this to store the average voltage on the capacitor. The capacitor is pre-charged to $195V$.

Now this entire unit from the input voltage source to the capacitor bank is equivalent to one CCVS. This can now be modulated using another IGBT bridge at the output, providing the required variable output voltage to the motor.

3.3.2 Control System

There are two control systems implemented, one for the input side and the other for the output side.

3.3.3 Input Control System

The current flowing through the inductor at the secondary of the transformer is filtered using a first-order Butterworth filter with a cutoff frequency of $2000Hz$. This is given as the feedback signal to the inner current controller loop. The voltage across the capacitor is fed back to the outer voltage controller loop. This system limits the average inductor current to a maximum value of $15A$, while trying to maintain the capacitor voltage at $195V$. The system is as shown in Figure 3.9. The K_p and K_i values for this controller were determined using **Ziegler-Nichols tuning method** and then further fine-tuned to achieve desirable performance.

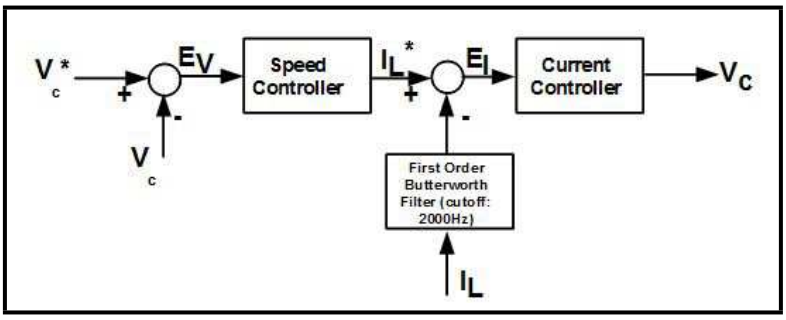

Figure 3.9: Working Topology: Input Control System

The output V_c generated is limited between $0V$ and $10V$. This(and its negative) is then compared with the bipolar triangular wave and given to the switch pairs as discussed earlier.

This input side control system limiting the secondary side rms current to $15A$ (implying primary side rms current being limited to $162.5A$) is what makes it practically implementable. In the previous topology, the solid-state devices in the H-bridge inverter were to withstand a maximum rms current of $750A$, but now it is reduced by almost 4.5 times. Therefore the number of devices to be put in parallel is reduced, thereby reducing the area of occupation if the entire system.

3.3.4 Output Control System

The output control system is similar to what was discussed earlier in the case of old topology, taking ω_m and I_a as the feedback signals with a few changes. As was explained earlier, the requirement is that the resultant voltage waveform be strictly unipo-

lar in one period of operation, not bipolar. Hence the switching strategy shown in Figure 3.10 is implemented. The control system generates a bipolar voltage signal V_c ranging from $-5V$ to $5V$. The absolute value and the sign of this signal is taken and based on the sign, switch pairs are activated. The resultant switching waveforms and armature voltages are as shown in Figure 3.11.

- Positive Output Voltages: The resultant V_c is positive. Switch pair $S7, S8$ is maintained in OFF state throughout the required period. $S6$ is kept ON throughout while $S5$ is operated by comparison of the absolute of V_c with the ramp voltage(varying between $0V$ and $5V$).
- Negative Output Voltages: The resultant V_c is negative. Switch pair $S5, S6$ is maintained in OFF state throughout the required period. $S8$ is kept ON throughout while $S7$ is operated by comparison of the absolute of V_c with ramp voltage.

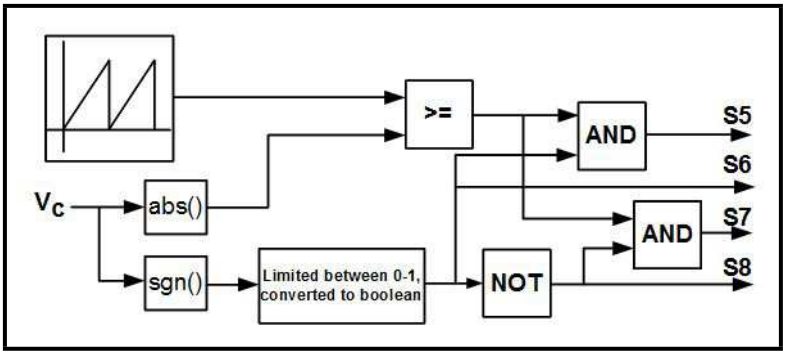

Figure 3.10: Working Topology: Output Switching Scheme

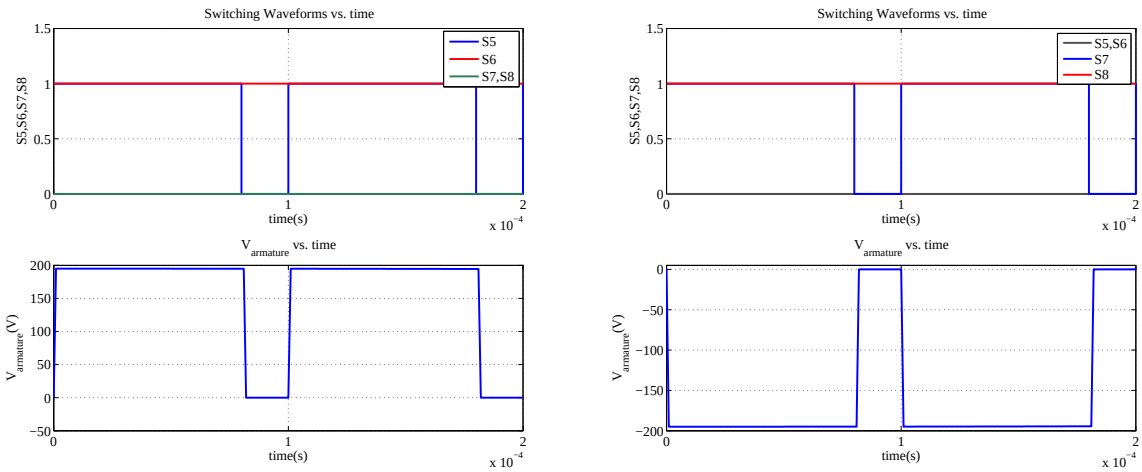

(a) For Positive Output Voltages

(b) For Negative Output Voltages

Figure 3.11: Output Bridge: Switching Waveforms

3.3.5 Regenerative Braking Switch

During braking, charge is sent back to capacitor leading to an increase in the voltage across the capacitor. For safe operating conditions, this voltage mustn't be allowed to rise to dangerous levels. Therefore the capacitor voltage is continuously monitored and the difference between the capacitor instantaneous voltage and the reference voltage(195V in this case) is sent to a LUT, where each value of difference corresponds to a specific duty ratio of the braking switch, as shown in Table 3.2.

Table 3.2: Braking Switch Operation Control

ΔV(V)	D
0	0
5	0
35	1

The values for other points is obtained by interpolation(within the rage) and extrapolation(outside the range). This is then compared with a ramp signal of frequency 10kHz and in the range $0V$ to $1V$, and the resultant pulses control the switching of the braking switch. The switch could have been directly turned completely ON/OFF, without a LUT, but that could lead current surges, which is not preferred for safety reasons.
This is as shown in Figure 3.12.

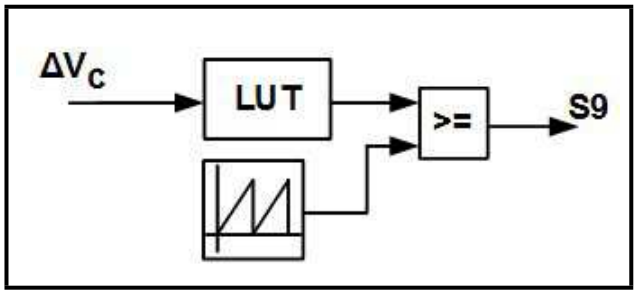

Figure 3.12: Regenerative Braking Switching Scheme

3.3.6 Simulation Results

The simulation results to show that the converter developed can indeed achieve four-quadrant operation, are as given below.

- Varying Speed and Constant Load = 1.68N.m
  This simulation was run at optimum accelerating/decelerating conditions, 200m/s^3. The results are as shown in Figure 3.13.
  1. Figure 3.13(a) shows the motor speed, ω_m and armature current, $I_{armature}$ profiles. It is seen that ω_m follows the reference voltage, ω_m^*, sincerely and $I_{armature}$ is well restricted within the specified limits and exhibits the expected pattern.
  2. Figure 3.13(b) shows the capacitor voltage and secondary current profiles. The capacitor voltage dips initially to $190V$ from $195V$, in the process of activating the inner loop. It then remains at $195V$ throughout, till $t = 1s$ when it rises to $200V$. This is because the ω_m has overshot and gone greater than ω_m^* and the current must reverse direction to apply a reverse torque to brake the system and bring it down to ω_m^*. At $t = 2s$, the huge rise in voltage to $372V$ is because the current has to remain negative(charge pumped back to the capacitor) throughout the period $t = 2s$ to $t = 3.5s$, to first brake the system and then reverse the direction of rotation. But the regenerative braking switch swings into action and the voltage rise is brought under control by $t = 2.45s$. A similar rise to $200V$ is observed at $t = 2.5s$, due to a slower rate of acceleration in the reverse direction, thereby causing excess energy to be returned to the capacitor. Similar explanation follows for the later period. The secondary current is well restricted within the specified limits and exhibits the expected pattern.
  3. Figure 3.13(c) shows the torque profile and current through the regenerative braking circuit. The electromechanical torque generated by the motor in sense, is a scaled down version of the current profile, . $J\frac{d\omega_m}{dt} = T_e - T_L - B\omega_m$ gives that at steady state non-zero speeds, the generated electromechanical torque is higher/lower(depending on the sign of ω_m) by the load torque by a factor of $B\omega_m$. The current flowing through the braking resistor, shows a jittering pattern between $t = 3.5s$ and $t = 4.8s$ as the switch is operated with a particular duty ratio, but since a practical motor operates in the braking mode for a short time, this jittering dies down as the motor comes out of that mode, as is shown in the figure.

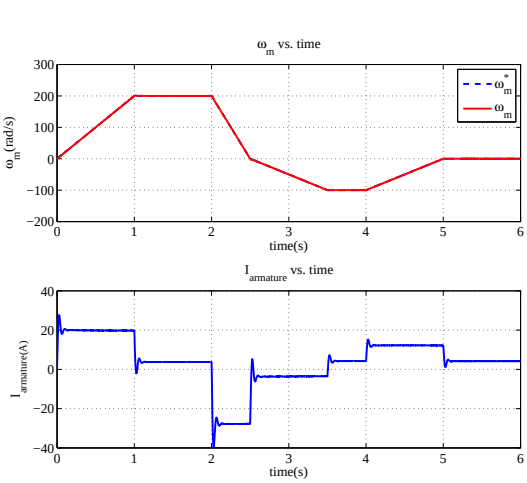

(a) Motor Speed and Current

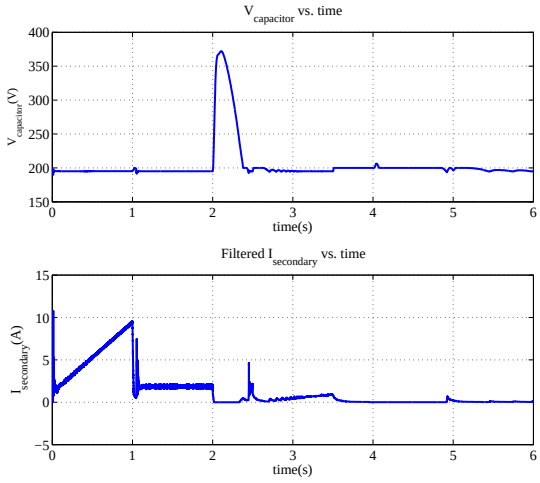

(b) Capacitor Voltage and Secondary Current

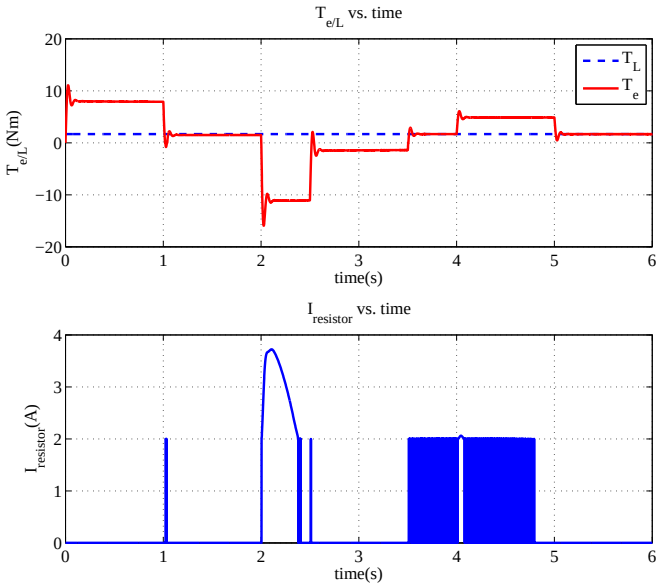

(c) Torque and Current through Braking Resistor

Figure 3.13: Varying Speed, Constant Torque: Drive Performance

- Varying Torque and Constant Speed = 205 rad/s The results are as shown in Figure 3.14.
  1. Figure 3.14(a) shows that motor speed, ω_m follows the reference voltage, ω_m^* sincerely. $I_{armature}$ is well restricted within the specified limits and varies in a manner so as to provide the required electromechanical torque.
  2. Figure 3.13(b) shows the capacitor voltage and secondary current profiles. The capacitor voltage dips to $190V$ initially, for reasons explained earlier. There is a small rise in voltage at $t = 1s$, due to reverse current flowing to brake the system to bring ω_m to ω_m^*. The capacitor voltage keeps rising after $t = 4s$ because the motor is in braking mode, but again we see the regenerative switch coming into action and bring the voltage down by $t = 5.75ss$. The secondary current is well limited within the specified limits and exhibits the expected pattern.

3. Figure 3.13(c) shows the torque profile and current through the regenerative braking circuit. The electromechanical torque generated by the system follows the load torque profile(with an offset of $B\omega_m$) after the speed has settled down since now $\frac{d\omega_m}{dt} = 0$. The jittering, as observed earlier, dies down when the motor comes out of the braking mode.

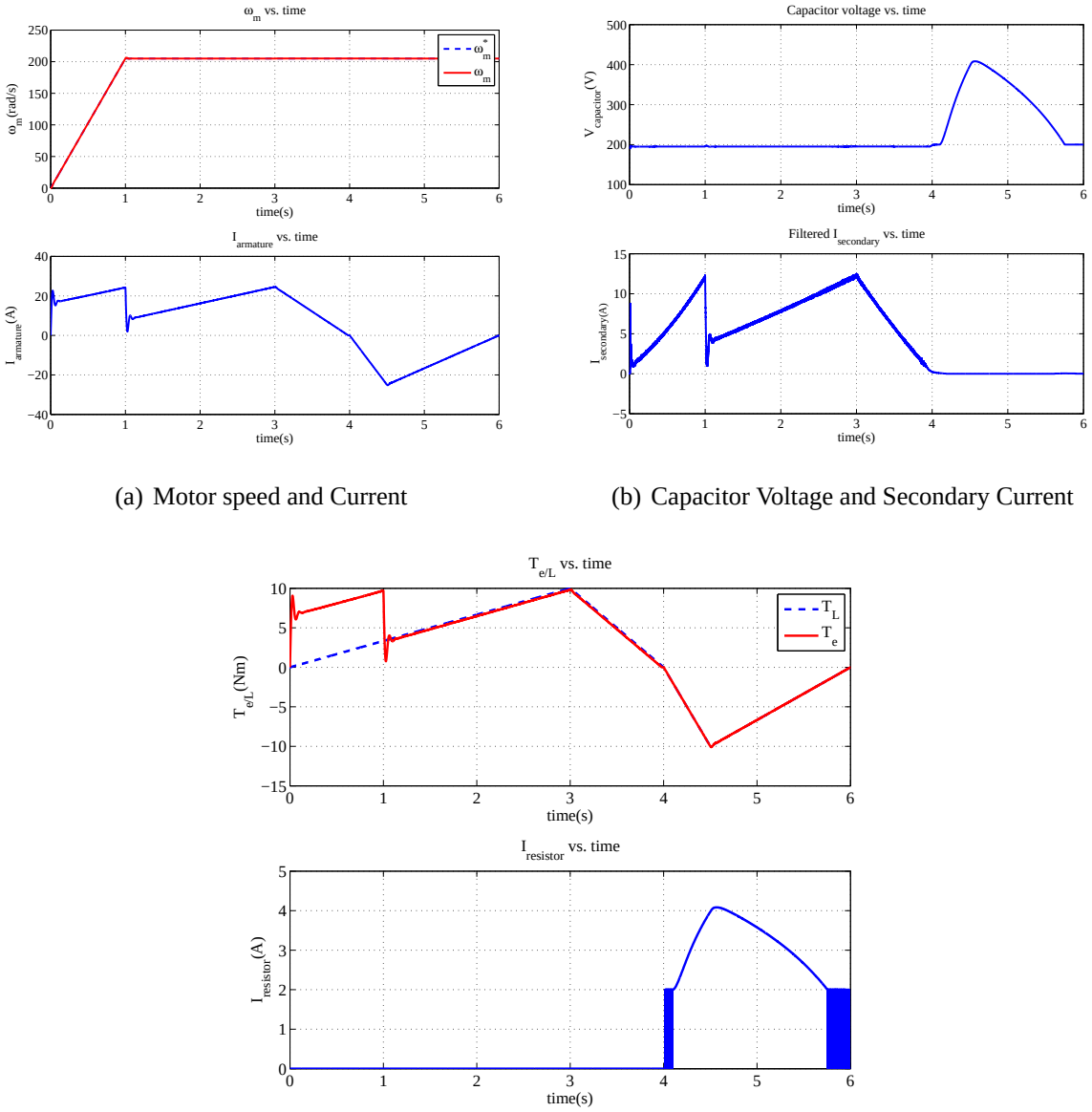

(a) Motor speed and Current

(b) Capacitor Voltage and Secondary Current

(c) Torque and Current through Braking Resistor

Figure 3.14: Varying Speed, Constant Torque: Drive Performance

These results verify that the converter developed is a four-quadrant drive for the given DC motor. The control systems help system perform desirably. The speed overshoot is 5% and the settling time is 1.1s making it suitable for practical applications.

CHAPTER 4

HARDWARE IMPLEMENTATION

The hardware implementation is done for lab prototype with the system parameters as given in Table 4.1.

Table 4.1: Motor Parameters

N_{rated}	3000rpm
V_{rated}	83V
P_{rated}	1kW
I_{rated}	14.4A

$V_{input} = 40V$ for this system. The lab prototype circuit diagram is as shown in Figure 4.1.

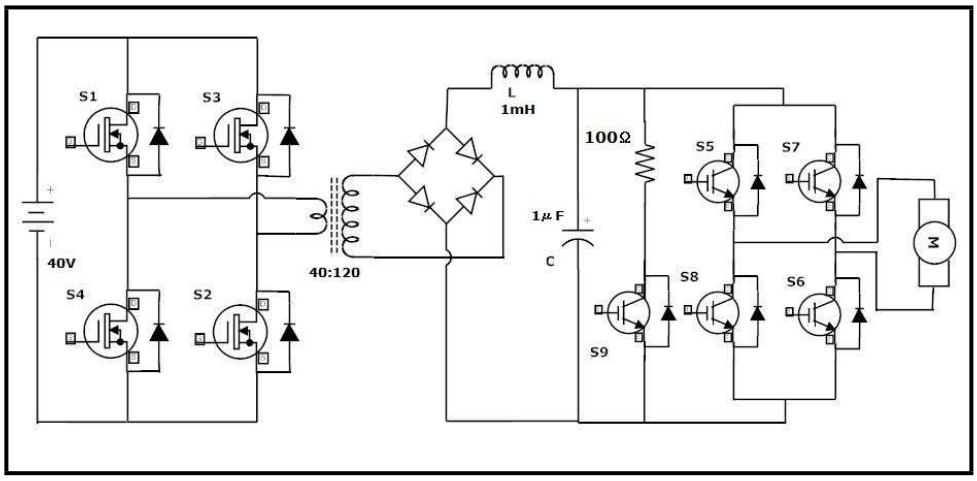

Figure 4.1: Lab Prototype

The implementation must be done in the following stages:

1. Identifying and obtaining suitable devices.
2. Designing the PCB.

3. Designing the magnetic components.
4. Testing and verification of functionality:
   (a) Implementation of the control systems in DSP TMS320F2812.
   (b) Winding the transformer and inductor and verifying their performance.
   (c) Populating the board and testing to verify its functionality.

Two isolated power supplies each of $+15V$ need to be derived for the two driver boards. For this, a $230:18$ transformer with two secondary windings is being used. LM7815 regulates this resultant voltage to $+15V$. An LC filter is being added at the input to protect the voltage source from damages caused by high frequency switching ripples.

4.1 Identification of Suitable Devices

The following devices were selected for the hardware implementation.

1. MOSFETs: IRF3710 (TO-242).
2. Diodes: U30D40 (TO-242).
3. MOSFET Driver: IR2110 (14-Lead PDIP).
4. Optocoupler: HCPL2531 (8-Lead DIP).
5. Optocoupler-cum-Driver: TLP250 (8-Lead DIP).
6. IGBTs: G20N60B (TO-242).
7. Voltage Regulator: LM7815 (TO-220).

4.2 PCB Designing

The PCB designing was done using DipTrace for the lab prototype. The two types of boards developed were for:

1. Input and output power boards, as shown in Figure 4.2.
2. Input and output driver boards, as shown in Figure 4.3.

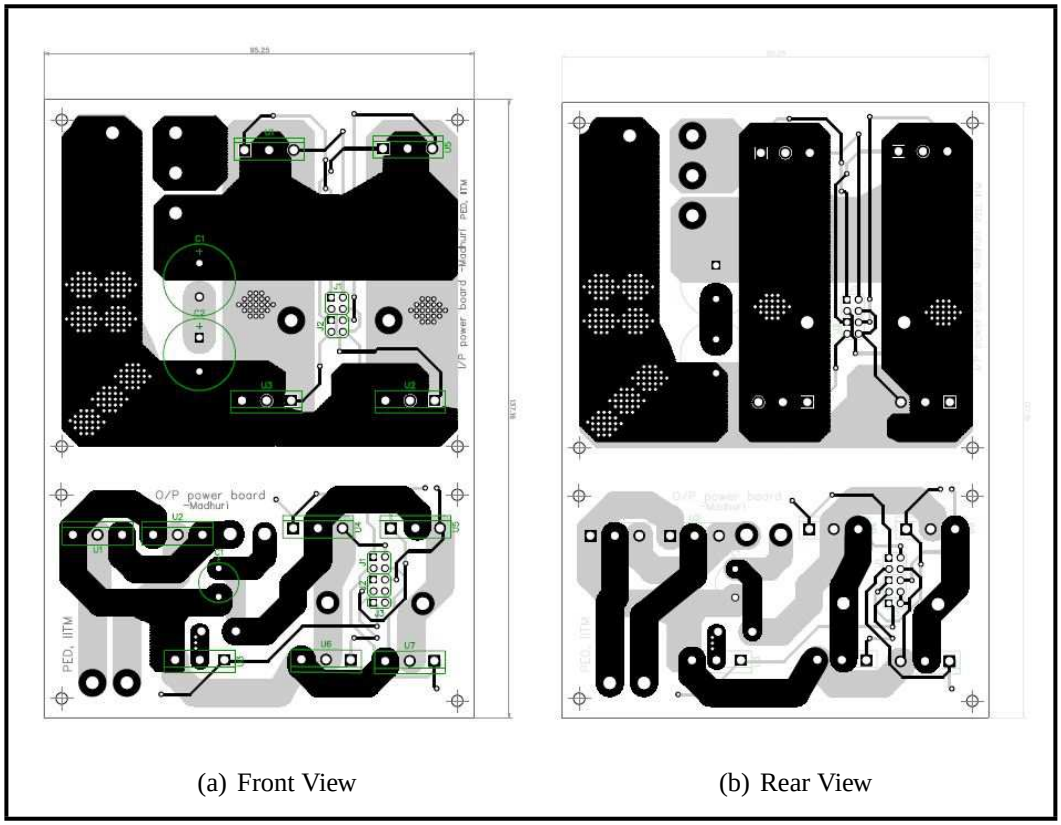

(a) Front View (b) Rear View

Figure 4.2: Input and Output Power Boards

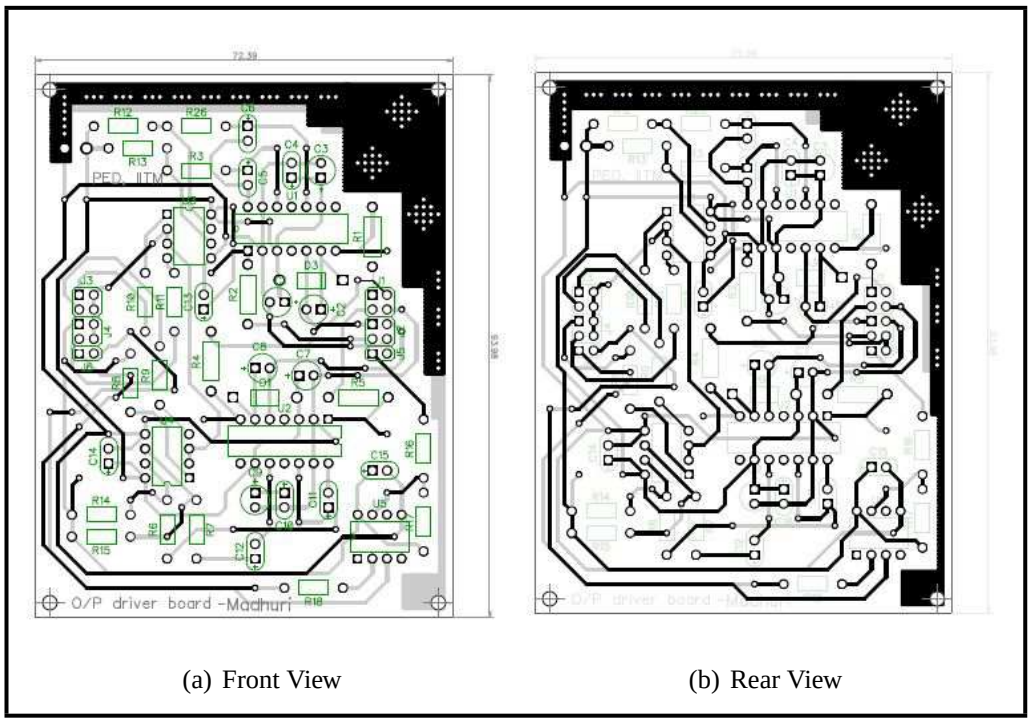

(a) Front View (b) Rear View

Figure 4.3: Input and Output Driver Boards

4.3 Designing the Magnetic Components

4.3.1 Inductor Design Equations

With L, I_{peak}, I_{rms}, k_w, B_m, J, core tables and SWG table as the input data, the following steps are followed to design an inductor:

- Compute

$$A_c A_w(cm^4) = \frac{LI_{peak}I_{rms}}{k_w B_m J} \tag{4.1}$$

- Match the computed $A_c A_w$ with the core table data and select the core with $A_c A_w$ atleast 1.5 times the computed value.
- Get the $A_c(cm^2))$ and $A_w(cm^2)$ for the selected core.
- Compute

$$N = \frac{LI_p}{B_m A_c} \tag{4.2}$$

  Round it up to the nearest highest integer value.

- Compute

$$a_w(cm^2) = \frac{I_{rms}}{J} \tag{4.3}$$

  Select the nearest whole number wire gauge and the corresponding a_w from the wire table. One of the issues here is that the skin depth of Cu is 0.6mm, therefore choosing a wire with a diameter > 1.2mm would be improper use of resources.

- From the cross-sectional area of the selected wire (a_w^*), compute the number of strands needed to be put in parallel to carry the required current

$$N_{parallel} = \frac{a_w}{a_w^*} \tag{4.4}$$

  Round it up to the nearest highest integer value.

- Compute the air-gap

$$l_g(mm) = \frac{\mu_o N I_{peak}}{B_m} \tag{4.5}$$

- Verify the assumptions that core reluctance « air-gap reluctance and $l_g << \sqrt{A_c}$ (for no fringing).
- Recalculate

$$J^*(A/mm^2) = \frac{I_{rms}}{a_w^*} \tag{4.6}$$

  Ensure this is within a reasonable range, to avoid over-heating of the wires.

- Recalculate
$$k_w^* = \frac{N a_w^*}{A_w} \tag{4.7}$$
- Compute the AC flux in the air gap
$$B_{ac}(T) = \frac{0.4\pi(\Delta I/2)10^{-4}}{l_g(cm)} \tag{4.8}$$
- For the selected core, compute the surface area available. For Honeywell POWERLITE Amorphous C-Cores, this is calculated as
$$SA(cm^2) = 2f(b+d) + 2(b+d)(b+e) + 2f(b+e) \tag{4.9}$$
- Compute the mean turn length for the selected core
$$L_{MT}(cm) = 2(a+2b+d) \tag{4.10}$$
- For the selected wire, get the resistance per unit length(R_{ul}) and compute the total resistance for the N number of turns with $N_{parallel}$ strands in parallel
$$R_{wire}(\Omega) = \frac{R_{ul} N L_{MT}}{N_{parallel}} \tag{4.11}$$
- Compute the Cu losses given by
$$P_{Cu}(W) = I_{rms}^2 R_{wire} \tag{4.12}$$
- Obtain the weight of the selected core from the core table and compute the core loss as
$$P_{core}(W) = 6.5 f_{sw}^{1.51} B_{ac}^{1.74} wt \tag{4.13}$$
where fsw is in kHz and wt is in kg.
- Total power loss
$$P_{total}(W) = P_{Cu} + P_{core} \tag{4.14}$$
- Calculate the temperature rise of the core
$$\Delta T(^\circ) = \left(\frac{P_{total}(mW)}{SA(cm^2)}\right)^{0.833} \tag{4.15}$$
Ensure that this rise in temperature is within the acceptable range, which depends on the class of insulation that is being used. Here, we are using Class A insulation, which can support a maximum of 105 °C.

4.3.2 Inductors

The above-mentioned steps for designing the inductor were followed and the computation results are as listed in Table 4.2.

Table 4.2: Input and Output Inductor Computations

Computations	Input side inductor	Output side inductor
L	25μ H	1mH
I_{peak}(A)	45	15
I_{rms}(A)	36	12
J(A/mm^2)	2.5	2.5
B_m(T)	1	1
k_w	0.6	0.6
A_cA_w(computed)(cm^4)	2.7	12
A_cA_w(table)(cm^4)	3.92	24.13
Core	UMCCC-4	UMCCC-25
A_c(cm^2)	1.13	2.73
A_w(cm^2)	3.47	8.94
N	10(18 in parallel)	55(6 in parallel)
a_w(cm^2)	0.144	0.048
Wire Gauge	SWG19	SWG19
a_w^*(cm^2)	0.8171	0.8171
l_g(mm)	0.565	1.037
J^*(A/mm^2)	2.447	2.448
k_w^*	0.424	0.305
B_{ac}(T)	0.1	0.1
R_{wire}(mΩ)	1.112	20.882
P_{Cu}(W)	1.44	3.01
P_{core}(W)	0.37	1.43
P_{total}(W)	1.81	4.44
ΔT(°C)	11.89	12.15

4.3.3 Transformer Design Equations

With V, P_{rated}, $D_{optimum}$, k_w, B_m, J, f_s, core tables and SWG table as the input data, the following steps are followed to design a transformer:

- Compute

$$A_cA_w(cm^4) = \frac{2P_{rated}D_{optimum}}{4f_sB_mJk_w} \tag{4.16}$$

- Match the computed A_cA_w with the core table data and select the core with A_cA_w at least 1.5 times the computed value.
- Get the $A_c(cm^2)$ and $A_w(cm^2)$ for the selected core.
- Compute

$$N1 = \frac{P_{rated}D_{optimum}10^4}{4B_mA_cf_sk_w} \tag{4.17}$$

$$N2 = TR * N1 \tag{4.18}$$

where TR is the turns ratio of the transformer. Round these up to the nearest highest integer values.

- Compute

$$a_{w,p/s}(cm^2) = \frac{I_{rms,p/s}}{J} \tag{4.19}$$

Select the nearest whole number wire gauge and the corresponding a_w from the wire table. One of the issues here is that the skin depth of Cu is 0.6mm, therefore choosing a wire with a diameter > 1.2mm would be improper use of resources.

- From the cross-sectional area of the selected wire (a_w^*), compute the number of strands needed to be put in parallel to carry the required current for the primary side and the secondary side using

$$N_{parallel,p/s} = \frac{a_{w,p/s}}{a^*_{w,p/s}} \tag{4.20}$$

Round it up to the nearest highest integer value.

- Recalculate

$$k_w^* = \frac{A_{Cu}}{A_w} \tag{4.21}$$

where,

$$Acu = 0.008171((N_{parallel,p}N1) + (N_{parallel,s}N2)) \tag{4.22}$$

- For the selected core, compute the surface area available. For Honeywell POWERLITE Amorphous C-Cores, this is calculated as

$$SA(cm^2) = 2f(b+d) + 2(b+d)(b+e) + 2f(b+e) \tag{4.23}$$

- Compute the mean turn length for the selected core

$$L_{MT}(cm) = 2(a + 2b + d) \tag{4.24}$$

- For the selected wire, get the resistance per unit length(R_{ul}) and compute the total resistance for the N number of turns with $N_{parallel}$ strands in parallel

$$R_{wire,p/s}(\Omega) = \frac{R_{ul}NL_{MT}}{N_{parallel,p/s}} \tag{4.25}$$

- Compute the Cu losses given by

$$P_{Cu}(W) = I^2_{rms,p/s}R_{wire,p/s} \tag{4.26}$$

- Obtain the weight of the selected core from the core table and compute the core loss as

$$P_{core}(W) = 6.5f_{sw}^{1.51}B_m^{1.74}wt \tag{4.27}$$

where fsw is in kHz and wt is in kg.

- Total power loss

$$P_{total}(W) = P_{Cu} + P_{core} \tag{4.28}$$

- Calculate the temperature rise of the core

$$\Delta T(^{\circ}C) = (\frac{P_{total}(mW)}{SA(cm^2)})^{0.833} \tag{4.29}$$

Ensure that this rise in temperature is within the acceptable range, which depends on the class of insulation that is being used. Here, we are using Class A insulation, which can support a maximum of 105 °C.

Table 4.3: Transformer Computations

Variable	Value
V_p(V)	40
V_s(V)	120
P_{rated}(W)	1500
$D_{optimum}$	0.64
B_m	0.7T
A_cA_w(cm^4)(calculated)	4
A_cA_w(cm^4)(data)	5.312
Core	UMCCC-5
A_c(cm^2)	1.66
A_w(cm^2)	3.2
$N1$	5(18 in parallel)
$N2$	15(6 in parallel)
k_w^*	0.46
R_p(mΩ)	0.61
R_s(mΩ)	5.46
$P_{Cu,p}$(W)	0.55
$P_{Cu,s}$(W)	1.23
P_{core}(W)	20.26
P_{total}(W)	22.04
ΔT(°C)	87.04

4.3.4 Core Specifications

The cores selected for our implementation were Honeywell POWERLITE Amorphous C-Cores. They have a high saturation flux density of $1.56T$. Table 4.4 gives the specifications of the selected cores. Figure 4.4 shows the front and side views of the core.

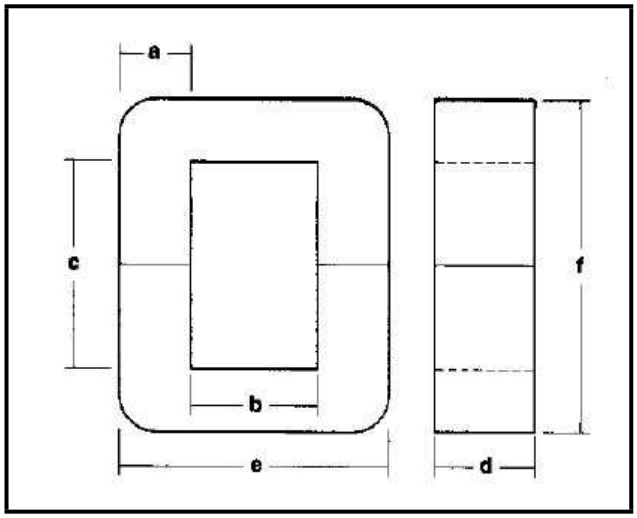

Figure 4.4: Core Front and Side Views

Table 4.4: Core Specifications

Property	a(mm)	b(mm)	c(mm)	d(mm)	e(mm)	f(mm)	L_{MT}(cm)	SA(cm^2)
UMCCC-4	9.5	11	34	15.5	30	52.4	9.4	92.47
UMCCC-5	10.4	10.2	34	20.5	31	54.3	10.26	103.38
UMCCC-25	13.8	16	58	25.5	43.6	84.8	14.26	220.93

CHAPTER 5

CONCLUSIONS

5.1 Conclusions

- Intensive simulations were performed to verify the performance of the converter as a four-quadrant drive to fine-tune its performance to achieve desirable results.
- The magnetic components were designed and suitable cores were procured to wind them.
- Suitable devices were identified and procured for the purpose of populating the PCB board.

5.2 Scope for Future Work

The near-future scope of this project is implementation of the control algorithm in TMS320F2812, verifying the performance of the magnetic components and testing the PCB boards. With these achieved, the amplidyne system can be replaced with the proposed solid-state system.

APPENDIX A

Control System Design

DC Motor control system design equations:

Voltage to current transfer function

$$\frac{I_a(s)}{V_a(s)} = \frac{Js + B}{s^2 JL_a + s(L_a B + R_a J) + (R_a B + (L_{af} I_f)^2)} \tag{A.1}$$

Armature time constant $\tau_a = \frac{L_a}{R_a} = 7.69\text{ms}$

Mechanical time constant $\tau_m = \frac{J}{B} = 0.89\text{hr}$

A.1 Current Loop Design

Converter transfer function

$$\frac{V_a(s)}{V_c(s)} = \frac{K_r}{1 + s\frac{T}{2}} \tag{A.2}$$

Plant transfer function : Converter*Voltage-to-current

$$\frac{I_a(s)}{V_a(s)} = \frac{1.08e08s + 33750}{s^3 + 20130s^2 + 2.601e06s + 2.008e07} \tag{A.3}$$

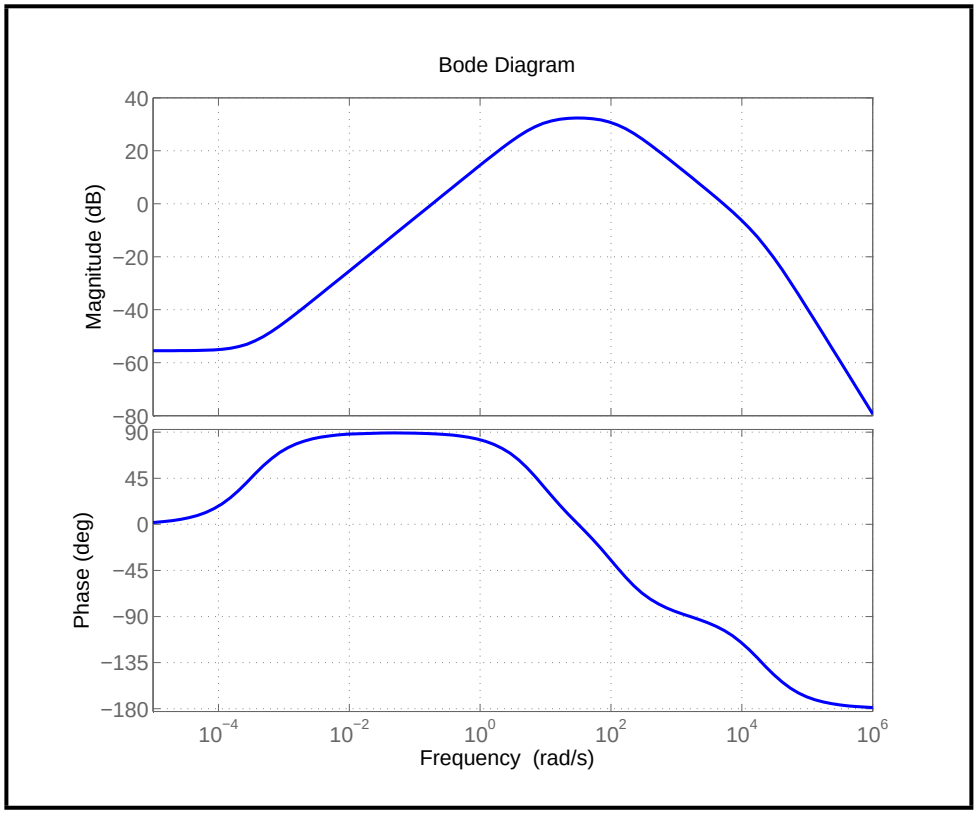

Figure A.1: Open Loop Frequency Response (Current)

Current controller transfer function For $1kHz$ BW

$$\frac{V_c(a)}{E_i(s)} = K_i + \frac{K_p}{s} = 1.37 + \frac{700}{s} \tag{A.4}$$

Current loop closed loop transfer function

$$\frac{I_a(s)}{I_a^*(s)} = \frac{\frac{V_c(a)}{E_i(s)} * \frac{I_a(s)}{V_a(s)}}{1 + \frac{V_c(a)}{E_i(s)} * \frac{I_a(s)}{V_a(s)}} = \frac{1.48e08s^2 + 7.56e10s + 2.362e07}{s^4 + 2.013e04s^3 + 1.506e08s^2 + 7.562e10s + 2.363e07} \tag{A.5}$$

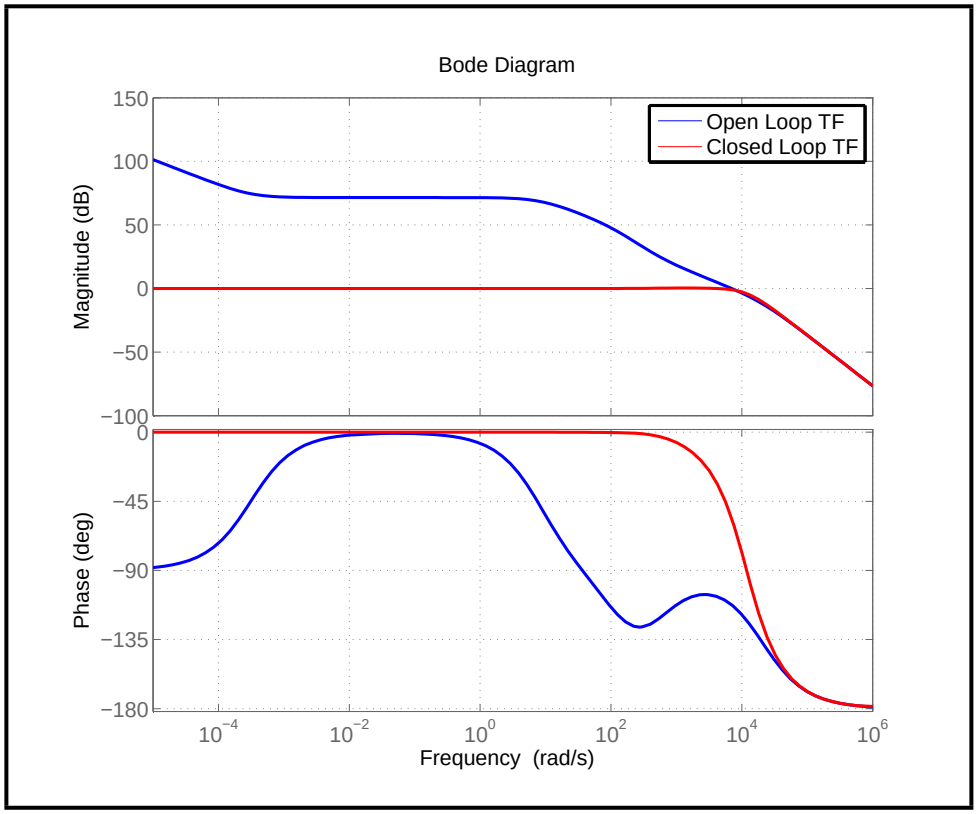

Figure A.2: Frequency Responses (Current)

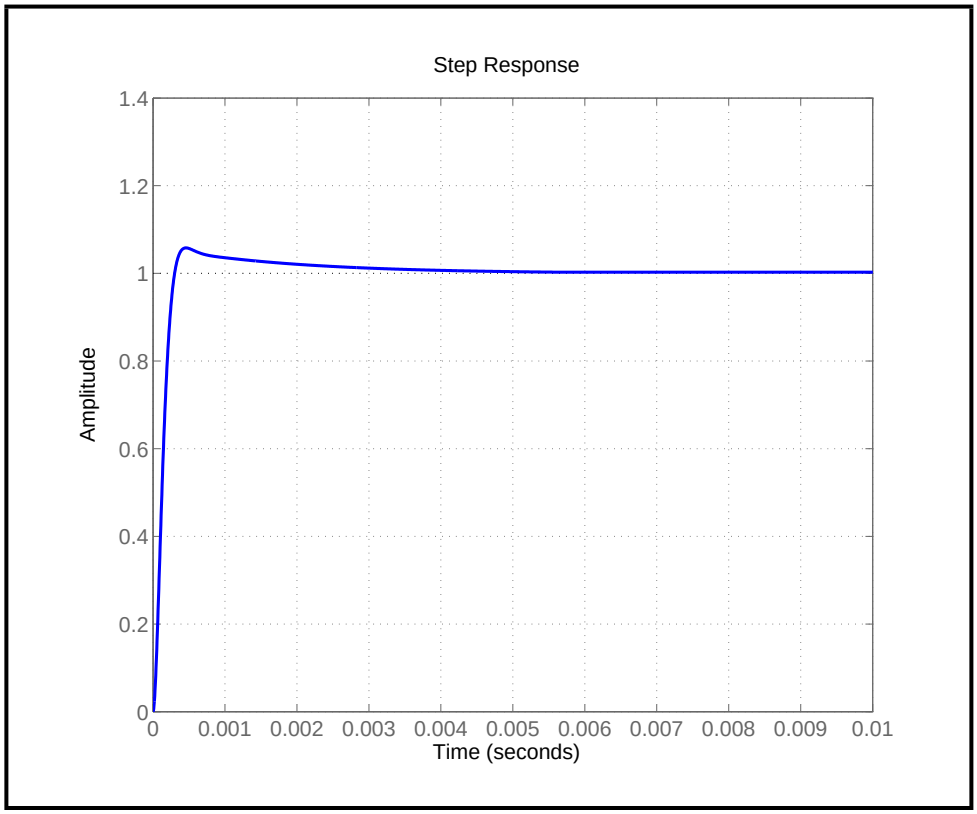

Figure A.3: Loop Step Response (Current)

A.2 Speed Loop Design

Mechanical system transfer function

$$\frac{\omega_m(s)}{I_a(s)} = \frac{L_{af} I_f}{Js + B} = \frac{0.4}{0.032s + 10^{-5}} \tag{A.6}$$

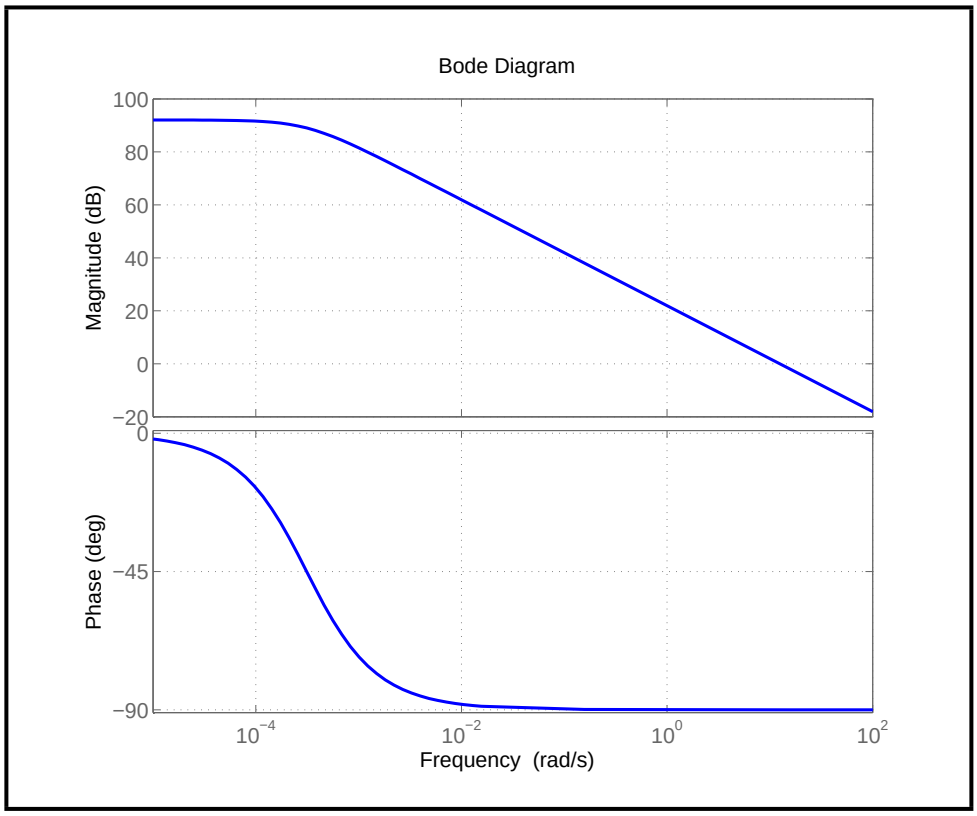

Figure A.4: Mechanical System

Speed controller transfer function For $100Hz$ BW

$$\frac{I_a^*(s)}{E_\omega(s)} = 30.2 + \frac{700}{s} \tag{A.7}$$

The K_p value was lated fine tuned to 5.73.

Speed loop closed loop transfer function

$$\frac{\omega_m(s)}{\omega_m^*(s)} = \frac{\frac{\omega_m(s)}{I_a(s)} * \frac{I_a^*(s)}{E_\omega(s)}}{1 + \frac{\omega_m(s)}{I_a(s)} * \frac{I_a^*(s)}{E_\omega(s)}} = \frac{12500s^3 + 8754s^2 + 2.734s}{s^4 + 1.25e04s^3 + 8754s^2 + 2.734s} \tag{A.8}$$

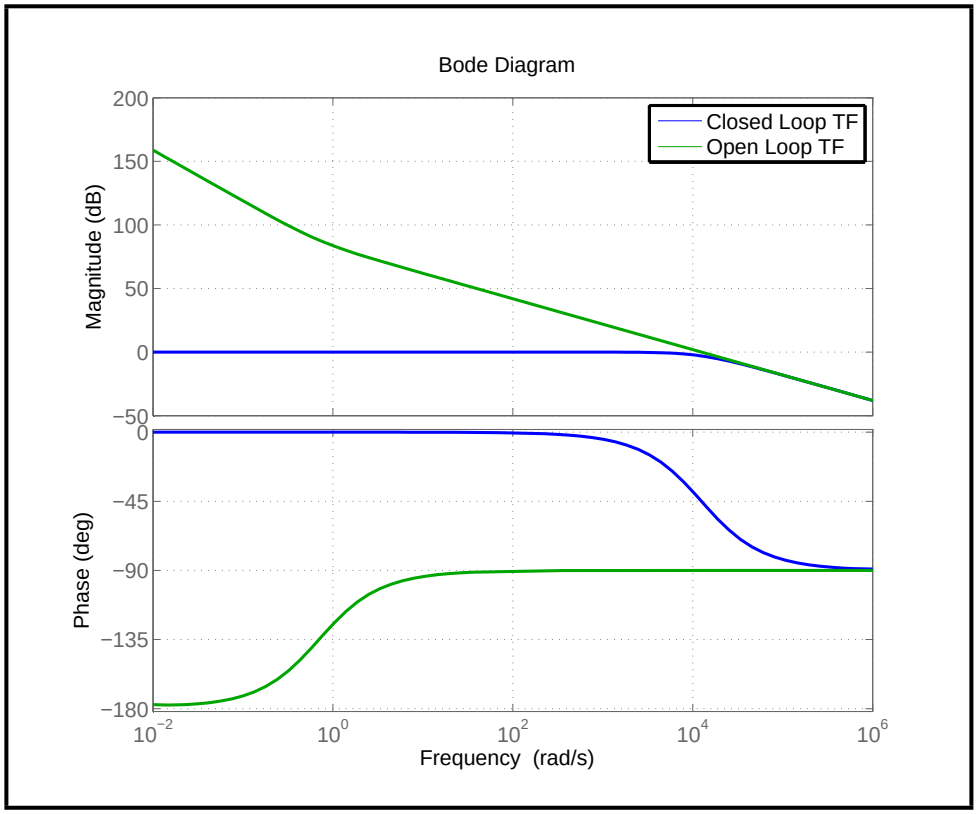

Figure A.5: Frequency Responses (Current)

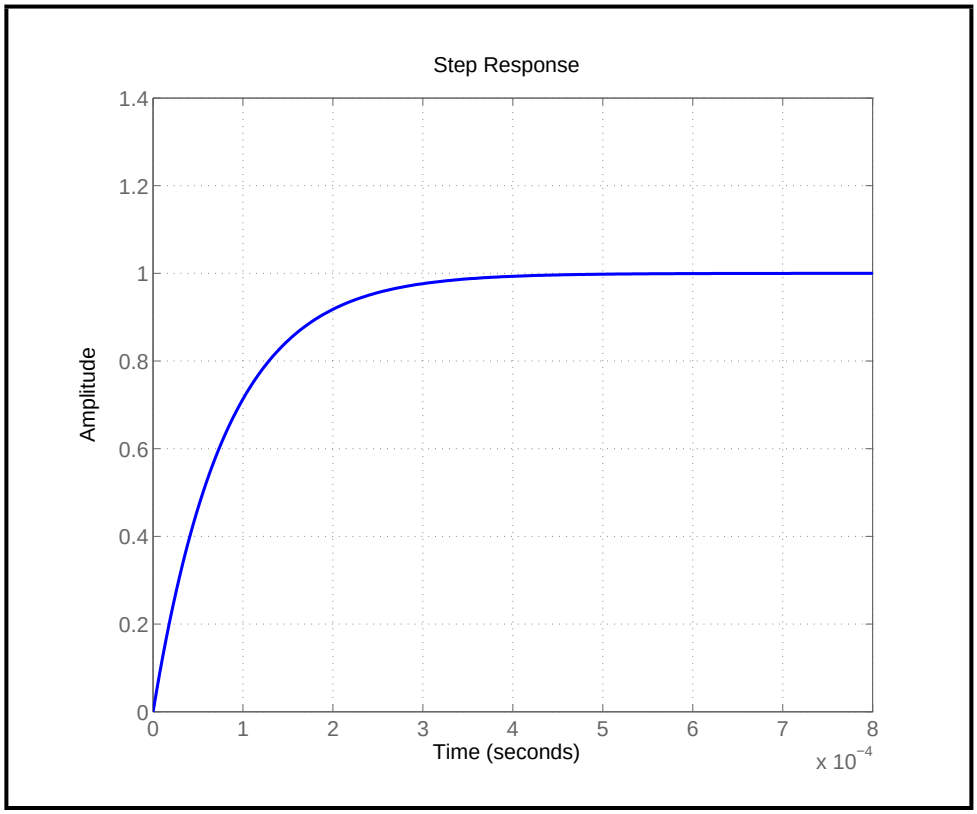

Figure A.6: Loop Step Response (Current)

REFERENCES

[1] R. Krishnan. *Electric Motor drives: Modelling, Analysis and Control*, Prentice Hall, Upper Saddle River, New Jersey, Third Edition, 2002.

[2] D.P Kothari, I.J Nagrath. *Electric Machines*, Tata McGraw-Hill Publishing Company Limited, Third Edition,2008.

[3] R.K. Rajput. *Electrical Machines*, Laxmi Publications (P) Limited, Third Edition, 2002.

[4] Technical datasheets provided by TI for DSP TMS320F2812.

[5] Application Guide provided by MetGlas POWERLITE - *http://download.21dianyuan.com/download.php?id=32275*.

[6] Drawing Tool: Smart Draw 2014.

[7] Google and Wikipedia.